Numerical Solutions of Peristaltic Flow of a Newtonian Fluid under the Effects of Magnetic Field and Heat Transfer in a Porous Concentric Tubes

Sohail Nadeem, Noreen Sher Akbar, and Muhammad Yousaf Malik

Department of Mathematics, Quaid-i-Azam University 45320, Islamabad 4400 Pakistan

Reprint requests to S. N.; E-mail: snqau@hotmail.com

Z. Naturforsch. **65a,** 369 – 380 (2010); received September 17, 2008 / revised June 4, 2009

In the present article, we have studied the effects of heat transfer on a peristaltic flow of a magnetohydrodynamic (MHD) Newtonian fluid in a porous concentric horizontal tube (an application of an endoscope). The problem under consideration is formulated under the assumptions of long wavelength and neglecting the wave number. A closed form of Adomian solutions and numerical solutions are presented which show a complete agreement with each other. The influence of pertinent parameters is analyzed through graphs.

Key words: Peristaltic Flow; Newtonian Fluid; Magnetic Field; Heat Transfer; Porous Concentric Tubes.

1. Introduction

Peristaltic transport is a form of fluid transport generated by a progressive wave of area contraction or expansion along the length of a distensible tube containing a fluid. This mechanism of fluid transport has received a considerable attention in recent times in engineering as well as in physiological science. These physiological and engineering applications include urine transport in the ureter, the motion of spermatozoa in the cervical canal, bile in the bile duct, etc. Engineering devices like finger pumps and roller pumps work on these principle. After the pioneering work of Latham [1], studies of the peristaltic flows in different flow geometries have been reported analytically, numerically, and experimentally by a number of researchers [2 – 14].

The study of heat transfer analysis in connection with peristaltic motion has industrial and biological applications, like sanitary fluid transport, blood pump in heart lung machine, and transport of corrosive fluids, where the contact of the fluid with the machinery parts is prohibited. The interaction of peristalsis and heat transfer has been recognized and has received some attentions [15 – 21] as it is thought to be relevant in some important processes such as hemodialysis and oxygination. Recently, Mekheimer and Abd Elmaboud [15] presented the influence of heat transfer and magnetic field on peristaltic transport of a Newtonian fluid in a vertical annulus. Vajravelu et al. [16] investigated the flow through a vertical porous tube with peristalsis and heat transfer. The difference between these two papers mentioned above is that Mekheimer and Abd Elmaboud [15] have consider the MHD term as a body force while Vajravelu et al. [16] have consider the porous medium term. The second main difference between these is that the authors of [15] have consider the energy equation without dissipation term whereas authors of [16] have consider the dissipation term as well as the porous medium contribution in the energy equation. In both papers [15, 16], the solution has been calculated using the perturbation method. There are various analytical methods to compute the solutions of the linear and nonlinear differential equations but each method has some limitations, for example the main draw back of the well-known perturbation method is that it is only valid if there arise some large or small parameter in the problem. Similarly, other methods have serious convergent problems. Recently, the Adomian decomposition method reached great importance [22 – 28]. If the closed form solution exists then one can easily discuss the convergence of the given problem.

Considering the importance of heat transfer in peristalsis and keeping in mind the sensitivity of convergence, an attempt is made to study the combined effects of heat transfer and magnetic field on peristaltic flow in a porous concentric horizontal tube. The flow is considered in the horizontal porous endoscope and a uniform magnetic field is applied in the transverse

direction to the flow. The non-dimensional problem is formulated in the wave frame under long wave length and low Reynolds number approximations. By using an Adomian decomposition method the closed form solutions for the velocity and temperature have been obtained. Furthermore, to check the validity of closed form Adomian solutions the governing equations are also solved numerical using finite difference scheme. Adomian solutions are found to be in complete agreement with the numerical results. In order to study the quantitative effects, graphical results are presented and discussed for different physical quantities.

2. Mathematical Formulation

We consider an electrically conducting flow of an incompressible Newtonian fluid through a porous region between two concentric tubes. A uniform magnetic field B_0 is applied in the transverse direction to the flow. Further, we consider the magnetic Reynolds number very small so that the induced magnetic field is negligible. We choose cylindrical coordinates (Z,R), where the Z-axis lies along the centre of the tube and R is transverse to it. The inner tube is maintained at temperature T_1 while the outer tube has the given temperature T_0. The inner tube has the radius a_1, while a_0 is the radius of the outer tube (see Fig. 1). The deformation of the outer tube wall due to the propagation of an infinite train of the peristaltic waves is represented by

$$R = H(Z,t) = a_0 + b\sin\left(\frac{2\pi}{\lambda}\right)(Z-ct), \qquad (1)$$

where b is the wave amplitude, λ is the wave length, c is the wave speed, and t is the time.

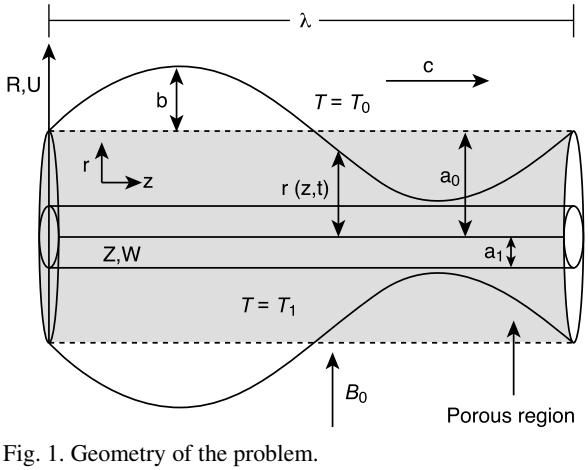

Fig. 1. Geometry of the problem.

The equations which govern the flow problem are defined as (for detail see [16])

$$0 = \frac{\partial W}{\partial Z} + \frac{U}{R} + \frac{\partial U}{\partial R}, \qquad (2)$$

$$0 = -\frac{\partial P}{\partial Z} + \frac{\mu}{R}\frac{\partial}{\partial R}\left(R\frac{\partial W}{\partial R}\right) - \frac{\mu}{K_0}W - B_0^2\sigma W, \qquad (3)$$

$$0 = \frac{k}{R}\frac{\partial}{\partial R}\left(R\frac{\partial T}{\partial R}\right) + \mu\left(\frac{\partial W}{\partial R}\right)^2 + \frac{\mu}{K_0}W^2 + B_0^2\sigma W^2, \qquad (4)$$

where W and U are velocity components of the fluid in Z and R directions, respectively, ρ is the density, μ is the variable viscosity, P is the pressure, k is the thermal conductivity, K_0 is the permeability of the porous medium, T is the temperature, B_0 is the magnetic field.

The boundary conditions are

$$W = 0 \text{ at } R = a_1, \qquad (5)$$

$$W = 0 \text{ at } R = H(z,t), \qquad (6)$$

$$T = T_1 \text{ at } R = a_1, \qquad (7)$$

$$T = T_0 \text{ at } R = H(z,t). \qquad (8)$$

The problem is simplified by using the following transformation and non-dimensional quantities

$$x = (Z - ct), \quad r = R, \quad w = W, \quad u = U, \qquad (9)$$

$$z = \frac{z}{\lambda}, \quad r = \frac{r}{a_0}, \quad w = \frac{w}{c}, \quad u = \frac{\lambda u}{a_0 c},$$
$$\theta = \frac{T - T_0}{T_1 - T_0}, \quad P = \frac{a_0^2}{\mu c \lambda}, \quad a_1 = \frac{a_1}{a_0}, \qquad (10)$$
$$\eta(z) = \frac{h(z)}{a_0}, \quad M = \sqrt{\frac{\sigma}{\mu}}B_0 a_1.$$

Making use of (9) and (10) and after dropping the prime, (2) to (8) take the following form:

$$0 = \frac{\partial w}{\partial z} + \frac{u}{r} + \frac{\partial u}{\partial r}, \qquad (11)$$

$$0 = -\frac{\partial P}{\partial z} + \frac{1}{r}\frac{\partial}{\partial r}\left(r\frac{\partial w}{\partial r}\right) - \alpha^2(w+1) - M^2(w+1), \qquad (12)$$

$$0 = +\frac{1}{r}\frac{\partial}{\partial r}\left(r\frac{\partial \theta}{\partial r}\right) + E_{\mathrm{m}}\left(\frac{\partial w}{\partial r}\right)^2 + \alpha^2 E_{\mathrm{m}}(w+1)^2 - M^2(w+1)^2. \qquad (13)$$

The relevant boundary conditions are

$$\begin{aligned} &w=-1, \text{ at } r=a_1,\\ &w=-1, \text{ at } r=\eta=1+\varepsilon\sin\pi z,\\ &\theta=1, \text{ at } r=a_1,\\ &\theta=0, \text{ at } r=\eta=1+\varepsilon\sin\pi z, \end{aligned} \tag{14}$$

where $\alpha^2 = a_0^2/K_0$ (Porosity parameter), $E_{\mathrm{m}} = c^2/k(T-T_0)$ (Eckert numbert), and $\varepsilon = b/a_0$ (amplitude ratio).

3. Exact Solution

The exact solution of (12) satisfying the first two equations of (14) can be written as

$$\begin{aligned} w=-1+\frac{\mathrm{d}P}{\mathrm{d}z}\frac{1}{\varphi^2}\{&\left[I_0(\varphi r)(K_0(\varphi a_1)-K_0(\varphi\eta))\right.\\ &\left.+I_0(\varphi r)(I_0(\varphi\eta)-I_0(\varphi a_1))\right]\\ \cdot&\left[I_0(\varphi\eta)K_0(\varphi a_1)-I_0(\varphi a_1)K_0(\varphi\eta)\right]^{-1}-1\}. \end{aligned} \tag{15}$$

4. Solution by Adomian Decomposition Method

According to the Adomian decomposition method, we write (12) in the operator form

$$L_r w = \frac{\mathrm{d}p}{\mathrm{d}z}+M^2+\alpha^2+M^2w+\alpha^2w$$

and this can be written as

$$L_r w = \frac{\mathrm{d}p}{\mathrm{d}z}+\varphi^2+(\varphi^2)w, \tag{16}$$

where

$$\varphi^2 = M^2+\alpha^2.$$

The differential operator L_r is defined in the form

$$L_r = \frac{1}{r}\frac{\partial}{\partial r}\left(r\frac{\partial}{\partial r}\right) \tag{17}$$

and the inverse operator L_r^{-1} is defined by

$$L_r^{-1}(.) = \int\left[\frac{1}{r}\int r(.)\mathrm{d}r\right]\mathrm{d}r. \tag{18}$$

Applying the inverse operator, (16) takes the form

$$w(r,z) = L_r^{-1}\left[\frac{\mathrm{d}p}{\mathrm{d}z}+\varphi^2+(\varphi^2)w\right]+c_1\ln r+c_2, \tag{19}$$

in which

$$\begin{aligned} &L_r^{-1}\left[\frac{\mathrm{d}p}{\mathrm{d}z}+\varphi^2+(\varphi^2)w\right] =\\ &\int\left[\frac{1}{r}\int r\left(\frac{\mathrm{d}p}{\mathrm{d}z}+\varphi^2+(\varphi^2)w\right)\mathrm{d}r\right)\mathrm{d}r. \end{aligned} \tag{20}$$

According to the Adomian decomposition method, we can write

$$w=\sum_{n=0}^{\infty} w_n.$$

Using the modified decomposition method, the solution $w(r,z)$ can be calculated by the recurrence relation

$$\begin{aligned} &w_0 = c_1\ln r+c_2,\\ &w_1 = L_r^{-1}\left[\frac{\mathrm{d}p}{\mathrm{d}z}+\varphi^2\right]+\varphi^2L_r^{-1}(w_0),\\ &w_{n+2} = \varphi^2L_r^{-1}(w_{n+1}), \quad n\geq 0, \end{aligned} \tag{21}$$

where c_1 and c_2 are constants.

The above equations give

$$\begin{aligned} w_1 &= \left(\frac{\mathrm{d}p}{\mathrm{d}z}+\varphi^2\right)\frac{r^2}{4}+\varphi^2\left(c_1\frac{r^3}{9}+c_2\frac{r^2}{4}\right),\\ w_2 &= \varphi^2\left(\frac{\mathrm{d}p}{\mathrm{d}z}+\varphi^2\right)\frac{r^4}{64}\\ &\quad+\varphi^4\left(c_1\frac{r^4\ln r}{64}-c_1\frac{3r^4}{128}+c_2\frac{r^4}{64}\right),\\ w_3 &= \varphi^4\left(\frac{\mathrm{d}p}{\mathrm{d}z}+\varphi^2\right)\frac{r^6}{2304}\\ &\quad+\varphi^6\left(c_1\frac{r^6\ln r}{2304}-c_1\frac{r^6}{4603}+c_2\frac{r^6}{2304}\right),\\ &\vdots\\ w_n &= \varphi^{2n-2}\left(\frac{\mathrm{d}p}{\mathrm{d}z}+\varphi^2\right)\frac{r^{2n}}{2^{2n}(n!)^2}\\ &\quad+\varphi^{2n}c_1\left(\frac{r^{2n}\ln r}{2^{2n}(n!)^2}\right)+\varphi^{2n}c_2\frac{r^{2n}}{2^{2n}(n!)^2},\\ &\quad n\geq 1. \end{aligned} \tag{22}$$

With the help of (21) and (22), the closed form of w can be written as

$$w(r,z) = w_0+\sum_{n=1}^{\infty} w_n$$

$$
\begin{aligned}
&= c_1 \ln r + c_2 \\
&+ \sum_{n=1}^{\infty} \left[\varphi^{2n-2} \left(\frac{\mathrm{d}p}{\mathrm{d}z} + \varphi^2 \right) \frac{r^{2n}}{2^{2n}(n!)^2} \right. \\
&\quad + \varphi^{2n} c_1 \left(\frac{r^{2n} \ln r}{2^{2n}(n!)^2} - \frac{r^{2n}}{2^{2n+1}(n!)^2} \right) \\
&\quad \left. + \varphi^{2n} c_2 \frac{r^{2n}}{2^{2n}(n!)^2} \right], \qquad (23)
\end{aligned}
$$

$$
\begin{aligned}
w(r,z) &= c_1 \left(1 + \sum_{n=1}^{\infty} \frac{(\varphi r)^{2n}}{2^{2n}(n!)^2} \right) \ln r - c_1 \sum_{n=1}^{\infty} \frac{r^{2n}}{2^{2n+1}(n!)^2} \\
&+ c_2 \left(1 + \sum_{n=1}^{\infty} \varphi^{2n} \frac{r^{2n}}{2^{2n}(n!)^2} \right) \qquad (24) \\
&+ \sum_{n=1}^{\infty} \varphi^{2n-2} \left(\frac{\mathrm{d}p}{\mathrm{d}z} \right) \frac{r^{2n}}{2^{2n}(n!)^2} + \sum_{n=1}^{\infty} \varphi^2 \frac{r^{2n}}{2^{2n}(n!)^2}.
\end{aligned}
$$

For the sake of simplicity, we can write (24) as

$$
\begin{aligned}
w(r,z) &= -1 + I_0(\varphi r) \\
&+ \frac{c_1}{2}(1 - I_0(\varphi r) + 2 I_0(\varphi r) \ln r) \qquad (25) \\
&+ c_2 I_0(\varphi r) + \frac{1}{\varphi^2} \frac{\mathrm{d}p}{\mathrm{d}z} (I_0(\varphi r) - 1),
\end{aligned}
$$

where $I_0(\varphi r)$ is a modified Bessel function of first kind,

$$
I_0(\varphi r) = \sum_{n=0}^{\infty} \frac{(\varphi r)^{2n}}{2^{2n}(n!)^2},
$$

and

$$
c_1 = \frac{\mathrm{d}p}{\mathrm{d}z} a_{20}, \quad c_2 = \frac{\mathrm{d}p}{\mathrm{d}z} a_{21} - 1,
$$

so

$$
\begin{aligned}
w(r,z) &= -1 \\
&+ \frac{\mathrm{d}p}{\mathrm{d}z} \left(\frac{a_{20}}{2}(1 - I_0(\varphi r) + 2 I_0(\varphi r) \ln r) \right. \qquad (26) \\
&\left. + I_0(\varphi r) a_{21} + \frac{1}{\varphi^2}(I_0(\varphi r) - 1) \right).
\end{aligned}
$$

The instantaneous volume flow rate in the fixed coordinate system is given by [11]

$$
Q = F + \frac{1}{2}\left(1 - a_1^2 + \frac{\phi^2}{2}\right). \qquad (27)
$$

The volume flow rate F in the moving frame is given by

$$
F = \int_{a_1}^{\eta} r w \mathrm{d}r. \qquad (28)
$$

Substitution of (26) in (28) and then solve the result for $\mathrm{d}p/\mathrm{d}z$ we have

$$
\frac{\mathrm{d}p}{\mathrm{d}z} = \frac{2F + (\eta^2 - a_1^2) - a_{23}}{a_{24}}. \qquad (29)
$$

Making use of (26) in (13) we can evaluate the expression for the temperature profile as

$$
\begin{aligned}
\theta(r,z) &= \sum_{m=0}^{\infty} \sum_{k=0}^{\infty} e_{mk} (\varphi r)^{2m+2k+4} \\
&+ \sum_{m=0}^{\infty} \sum_{k=0}^{\infty} f_{mk} (\varphi r)^{2m+2k+4} \ln r \\
&+ \sum_{m=0}^{\infty} \sum_{k=0}^{\infty} g_{mk} (\varphi r)^{2m+2k+3} \\
&+ \sum_{m=0}^{\infty} \sum_{k=0}^{\infty} h_{mk} (\varphi r)^{2m+2k+3} \ln r \\
&+ \sum_{m=0}^{\infty} \sum_{k=0}^{\infty} I_{mk} (\varphi r)^{2m+2k+2} \\
&+ \sum_{m=0}^{\infty} \sum_{k=0}^{\infty} J_{mk} (\varphi r)^{2m+2k+2} \ln r \qquad (30) \\
&+ \sum_{m=0}^{\infty} \sum_{k=0}^{\infty} K_{mk} (\varphi r)^{2m+2k+2} (\ln r)^2 \\
&+ \sum_{m=0}^{\infty} \sum_{k=0}^{\infty} L_{mk} (\varphi r)^{2m+2k+1} \\
&+ \sum_{m=0}^{\infty} \sum_{k=0}^{\infty} M_{mk} (\varphi r)^{2m+2k} \\
&+ \sum_{k=0}^{\infty} N_k (\varphi r)^{2k+1} + \sum_{k=0}^{\infty} O_k (\varphi r)^{2k+1} (\ln r)^2 \\
&+ \sum_{k=0}^{\infty} P_k (\varphi r)^{2k+2} + \sum_{k=0}^{\infty} Q_k (\varphi r)^{2k+2} \ln r \\
&+ b_1 \ln r + b_4.
\end{aligned}
$$

The corresponding stream functions ($u = -\frac{1}{r}\frac{\partial \Psi}{\partial z}$ and $w = \frac{1}{r}\frac{\partial \Psi}{\partial r}$) can be written as

$$
\begin{aligned}
\Psi(r,z) &= -\frac{r^2}{2} + \frac{\mathrm{d}p}{\mathrm{d}z} \left[\left(\frac{r}{\varphi^3} I_1(\varphi r) - \frac{r^2}{2\varphi^2} \right) \right. \\
&+ \frac{a_{20}}{2} \left(\frac{r^2}{2} - \frac{r}{\varphi} I_1(\varphi r) + \frac{2r}{\varphi} I_1(\varphi r) \ln r + \frac{2}{\varphi^2} - \frac{2 I_0(\varphi r)}{\varphi^2} \right) \\
&\left. + a_{21} \frac{r}{\varphi} I_1(\varphi r) \right]. \qquad (31)
\end{aligned}
$$

The pressure rise Δp and the friction force F_λ on inner

and outer tubes $F_\lambda^{(o)}$, $F_\lambda^{(i)}$, are given by

$$\Delta p_\lambda = \int_0^1 \frac{\mathrm{d}p}{\mathrm{d}z}\mathrm{d}z, \qquad (32)$$

$$F^{(o)} = \int_0^1 a_1^2\left(-\frac{\mathrm{d}p}{\mathrm{d}z}\right)\mathrm{d}z,\ F^{(i)} = \int_0^1 \eta^2\left(-\frac{\mathrm{d}p}{\mathrm{d}z}\right)\mathrm{d}z, \qquad (33)$$

where

$$a_3 = \varphi + \frac{\mathrm{d}p}{\mathrm{d}z}\frac{1}{\varphi} - \frac{a_1\varphi}{2}, \quad a_4 = a_1\varphi, \quad a_5 = -(\alpha^2 E_\mathrm{m} + M^2), \quad a_6 = 1 + \frac{\mathrm{d}p}{\mathrm{d}z}\frac{1}{\varphi^2} - \frac{a_1}{2} + a_2,$$

$$a_7 = -\frac{1}{\varphi^2} + \frac{a_1}{2}, \quad a_8 = -E_\mathrm{m}a_3^2, \quad a_9 = a_4^2, \quad a_{10} = a_1^2, \quad a_{11} = 2a_3a_4, \quad a_{12} = 2a_3a_1,$$

$$a_{13} = 2a_4a_1, \quad a_{14} = -(\alpha^2 E_\mathrm{m} + M^2)a_6^2, \quad a_{15} = a_7^2, \quad a_{16} = a_1^2, \quad a_{17} = 2a_6a_7, \quad a_{18} = 2a_6a_1,$$

$$a_{19} = 2a_7a_1, \quad a_{20} = \frac{2(I_0(\varphi a_1) - I_0(\varphi\eta))}{\varphi^2(I_0(\varphi a_1) + I_0(\varphi\eta) + 2I_0(\varphi a_1)I_0(\varphi\eta)\ln a_1 - 2I_0(\varphi a_1)I_0(\varphi\eta)\ln\eta)},$$

$$a_{21} = \frac{(-2I_0(\varphi a_1)\ln a_1(-1 + I_0(\varphi\eta)) + 2(-1 + I_0(\varphi a_1)I_0(\varphi a_1)I_0(\varphi\eta)))}{\varphi^2(I_0(\varphi\eta) + I_0(\varphi a_1) + 2I_0(\varphi a_1)I_0(\varphi\eta)\ln a_1 - 2I_0(\varphi a_1)I_0(\varphi\eta)\ln\eta)},$$

$$a_{mk} = \frac{1}{2^{2k+2m+2}k!(k+1)!2^{2m+1}m!(m+1)!}, \quad b_{mk} = \frac{1}{2^{2k+2m}(k!)^2(m!)^2},$$

$$c_{mk} = \frac{1}{2^{2k+2m+1}(k!)^2(m)!(m+1)!}, \quad d_k = \frac{1}{2^{2k}(k!)^2}, \quad e_{mk} = \frac{a_8 + 3a_9 + 2a_9/\varphi^2}{\varphi^2(2m+2k+4)^2},$$

$$f_{mk} = \frac{-2a_9}{\varphi^2(2m+2k+4)^3}, \quad g_{mk} = \frac{-a_{13} - a_{13}/\varphi}{\varphi^2(2m+2k+3)^3}, \quad h_{mk} = \frac{a_{13}}{\varphi^2(2m+2k+3)^2},$$

$$J_{mk} = \frac{-2a_{16}}{\varphi^2(2m+2k+2)^2}, \quad K_{mk} = \frac{a_{16}}{\varphi^2(2m+2k+2)^2}, \quad L_{mk} = \frac{a_{10}}{\varphi^2(2m+2k)^2},$$

$$M_{mk} = \frac{a_{11}}{\varphi^2(2m+2k+1)^3}, \quad N_k = \frac{a_{17}}{\varphi^2(2k+2)^2}, \quad O_k = \frac{-2a_{18}}{\varphi^3(2k+2)^3},$$

$$P_k = \frac{-2a_{18} - \varphi a_{19} - a_{19}\varphi^2}{\varphi^3(2k+2)^3}, \quad Q_k = \frac{-2a_{18} + a_{19}\varphi^2}{\varphi^3(2k+2)^3},$$

$$\begin{aligned}
b_1 = {} & \sum_{m=0}^{\infty}\sum_{k=0}^{\infty} e_{mk}(\varphi a_1)^{2m+2k+4} + \sum_{m=0}^{\infty}\sum_{k=0}^{\infty} f_{mk}(\varphi a_1)^{2m+2k+4}\ln r + \sum_{m=0}^{\infty}\sum_{k=0}^{\infty} g_{mk}(\varphi a_1)^{2m+2k+3} \\
& + \sum_{m=0}^{\infty}\sum_{k=0}^{\infty} h_{mk}(\varphi a_1)^{2m+2k+3}\ln r + \sum_{m=0}^{\infty}\sum_{k=0}^{\infty} I_{mk}(\varphi a_1)^{2m+2k+2} + \sum_{m=0}^{\infty}\sum_{k=0}^{\infty} J_{mk}(\varphi a_1)^{2m+2k+2}\ln a_1 \\
& + \sum_{m=0}^{\infty}\sum_{k=0}^{\infty} K_{mk}(\varphi a_1)^{2m+2k+2}(\ln a_1)^2 + \sum_{m=0}^{\infty}\sum_{k=0}^{\infty} L_{mk}(\varphi a_1)^{2m+2k+1} + \sum_{m=0}^{\infty}\sum_{k=0}^{\infty} M_{mk}(\varphi a_1)^{2m+2k} \\
& + \sum_{k=0}^{\infty} N_k(\varphi a_1)^{2k+1} + \sum_{k=0}^{\infty} O_k(\varphi a_1)^{2k+1}(\ln a_1)^2 + \sum_{k=0}^{\infty} P_k(\varphi a_1)^{2k+2} + \sum_{k=0}^{\infty} Q_k(\varphi r)^{2k+2}\ln a_1
\end{aligned}$$

$$\begin{aligned}
b_2 = {} & \sum_{m=0}^{\infty}\sum_{k=0}^{\infty} e_{mk}(\varphi\eta)^{2m+2k+4} + \sum_{m=0}^{\infty}\sum_{k=0}^{\infty} f_{mk}(\varphi\eta)^{2m+2k+4}\ln r + \sum_{m=0}^{\infty}\sum_{k=0}^{\infty} g_{mk}(\varphi\eta)^{2m+2k+3} \\
& + \sum_{m=0}^{\infty}\sum_{k=0}^{\infty} h_{mk}(\varphi\eta)^{2m+2k+3}\ln r + \sum_{m=0}^{\infty}\sum_{k=0}^{\infty} I_{mk}(\varphi\eta)^{2m+2k+2} + \sum_{m=0}^{\infty}\sum_{k=0}^{\infty} J_{mk}(\varphi\eta)^{2m+2k+2}\ln\eta \\
& + \sum_{m=0}^{\infty}\sum_{k=0}^{\infty} K_{mk}(\varphi\eta)^{2m+2k+2}(\ln a_1)^2 + \sum_{m=0}^{\infty}\sum_{k=0}^{\infty} L_{mk}(\varphi\eta)^{2m+2k+1} + \sum_{m=0}^{\infty}\sum_{k=0}^{\infty} M_{mk}(\varphi\eta)^{2m+2k} \\
& + \sum_{k=0}^{\infty} N_k(\varphi\eta)^{2k+1} + \sum_{k=0}^{\infty} O_k(\varphi\eta)^{2k+1}(\ln\eta)^2 + \sum_{k=0}^{\infty} P_k(\varphi\eta)^{2k+2} + \sum_{k=0}^{\infty} Q_k(\varphi\eta)^{2k+2}\ln\eta.
\end{aligned}$$

The non-dimensional expressions for the four considered wave forms are given by the following equations:

1. Sinusoidal wave:

$$h(z) = 1 + \phi \sin(2\pi z)$$

2. Triangular wave:

$$h(z) = 1 + \phi \left\{ \frac{8}{\pi^3} \sum_{n=1}^{\infty} \frac{(-1)^{n+1}}{(2n-1)} \sin(2\pi(2n-1)z) \right\}$$

3. Square wave:

$$h(z) = 1 + \phi \left\{ \frac{4}{\pi} \sum_{n=1}^{\infty} \frac{(-1)^{n+1}}{(2n-1)} \cos(2\pi(2n-1)z) \right\}$$

4. Trapezoidal wave:

$$h(z) = 1 + \phi \left\{ \frac{32}{\pi^2} \sum_{n=1}^{\infty} \frac{\sin\frac{\pi}{8}(2n-1)}{(2n-1)^2} \sin(2\pi(2n-1)z) \right\}.$$

5. Numerical Computations

A finite difference technique is employed to check the results of the perturbation analysis and to indicate their validity. Recall that the system of equations and boundary conditions in the long wavelength limit are given by

$$0 = -\frac{\partial p}{\partial z} + \frac{1}{r}\frac{\partial}{\partial r}\left(r\frac{\partial w}{\partial r}\right) - \varphi^2(w+1), \qquad (34)$$

$$\begin{aligned} &w = -1, \ \text{ at } \ r = a_1, \\ &w = -1, \ \text{ at } \ r = \eta = 1 + \varepsilon \sin 2\pi z, \end{aligned} \qquad (35)$$

where

$$\varphi^2 = M^2 + \alpha^2.$$

We use the finite difference method to solve the above equation treating it as an ordinary differential equation with the boundary conditions (35). The first step is to split the domain $[\alpha_1, \eta]$ into a number of sub-domains or intervals of length dr. We denote by r_i the interval end points or nodes with $r_1 = a_1$ and $r_{n+1} = \eta$. In general we have $r_i = (i-1)dr$ for $i = 1, 2, 3, \ldots, N$. We represent the axial velocity w at the ith node by w_i. The second step is to express the differential operators in a discrete form. This can be accomplished using finite difference approximations to the differential operators.

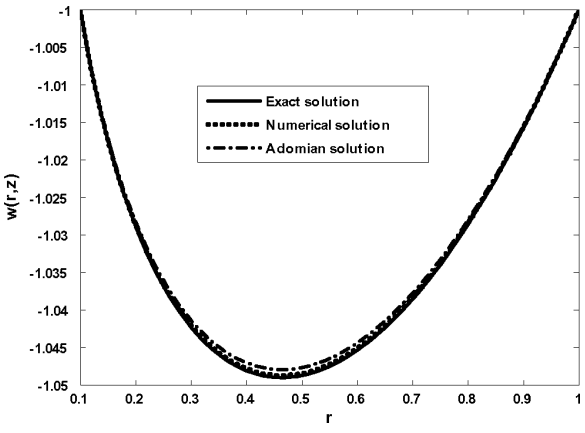

Fig. 2. Comparison of analytical and numerical solutions of the axial velocity w for $M = 0.8$, $a_1 = 0.45$, $\alpha = 0.2$, $\phi = 0.2$, $x = 0.5$.

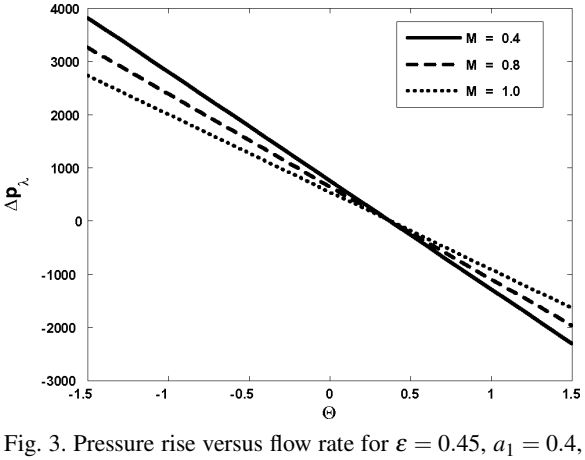

Fig. 3. Pressure rise versus flow rate for $\varepsilon = 0.45$, $a_1 = 0.4$, $\alpha = 0.8$.

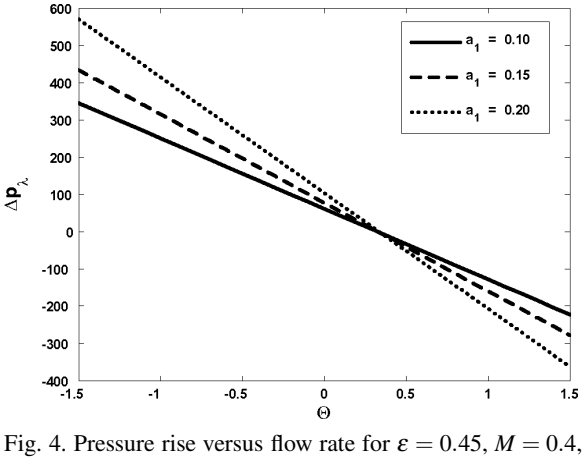

Fig. 4. Pressure rise versus flow rate for $\varepsilon = 0.45$, $M = 0.4$, $\alpha = 0.8$.

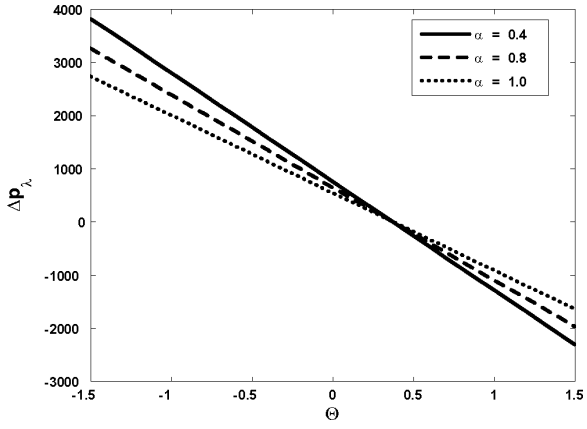

Fig. 5. Pressure rise versus flow rate for $\varepsilon = 0.45$, $M = 0.8$, $a_1 = 0.4$.

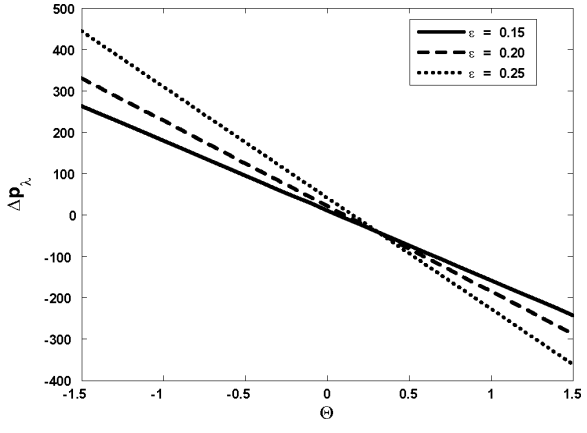

Fig. 6. Pressure rise versus flow rate for $M = 0.8$, $a_1 = 0.4$, $\alpha = 0.4$.

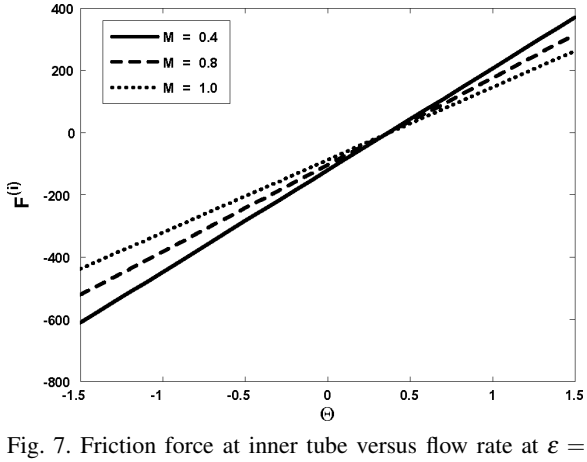

Fig. 7. Friction force at inner tube versus flow rate at $\varepsilon = 0.45$, $a_1 = 0.4$, $\alpha = 0.8$.

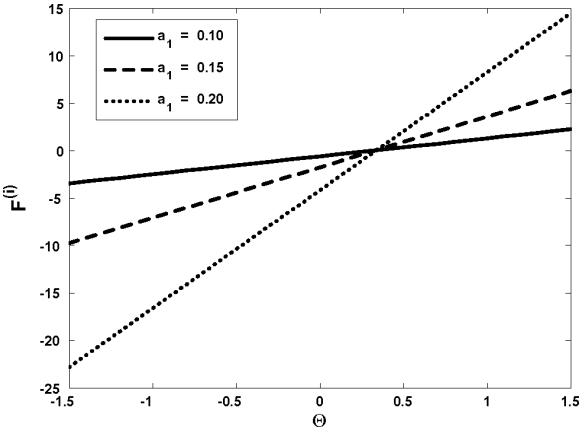

Fig. 8. Friction force at inner tube versus flow rate at $\varepsilon = 0.45$, $M = 0.4$, $\alpha = 0.8$.

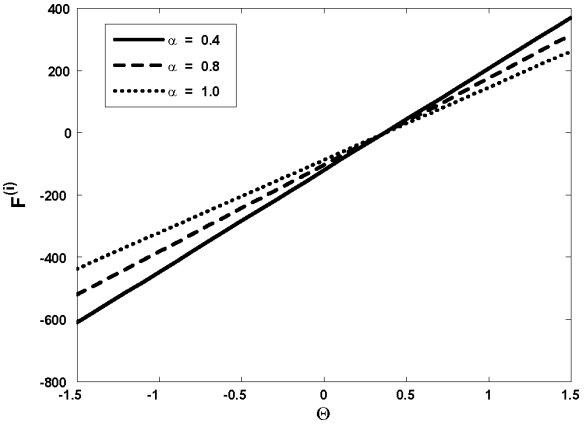

Fig. 9. Friction force at inner tube versus flow rate at $\varepsilon = 0.45$, $a_1 = 0.4$, $M = 0.8$.

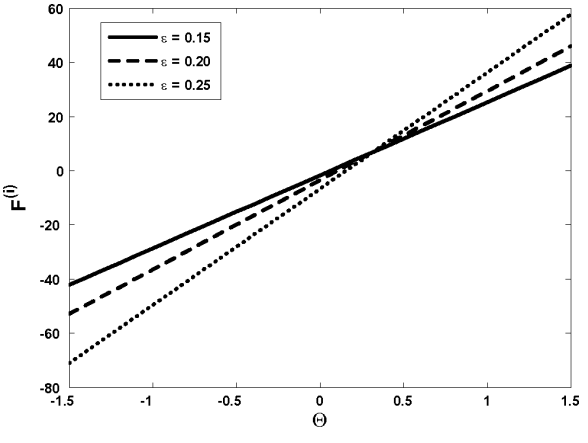

Fig. 10. Friction force at inner tube versus flow rate at $M = 0.8$, $a_1 = 0.4$, $\alpha = 0.4$.

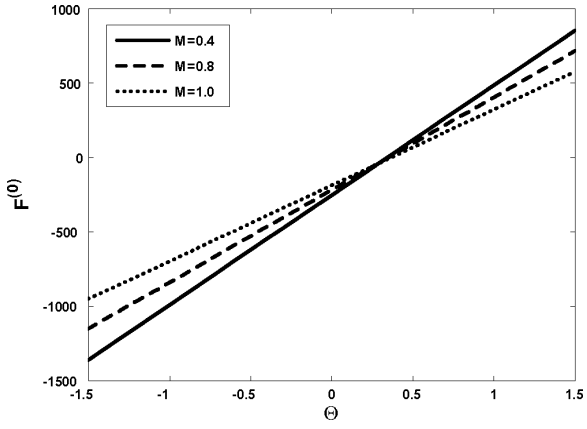

Fig. 11. Friction force at outer tube versus flow rate at $\varepsilon = 0.45$, $a_1 = 0.4$, $\alpha = 0.8$.

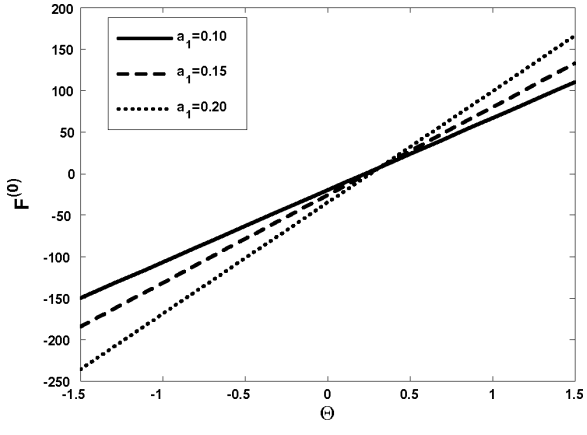

Fig. 12. Friction force at outer tube versus flow rate at $\varepsilon = 0.45$, $M = 0.4$, $\alpha = 0.8$.

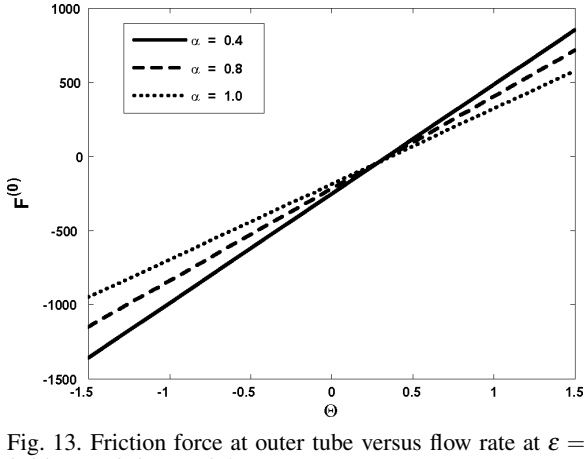

Fig. 13. Friction force at outer tube versus flow rate at $\varepsilon = 0.45$, $a_1 = 0.4$, $M = 0.8$.

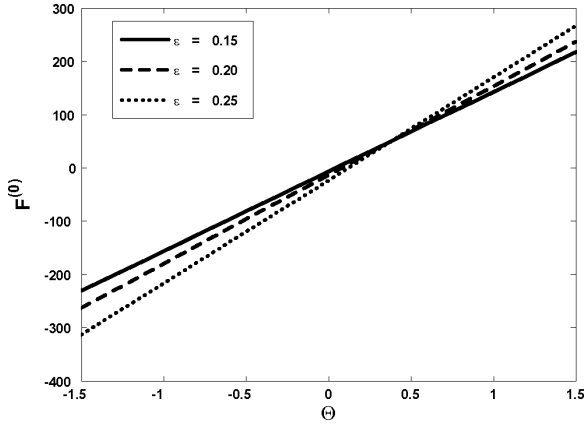

Fig. 14. Friction force at outer tube versus flow rate at $M = 0.8$, $a_1 = 0.4$, $\alpha = 0.4$.

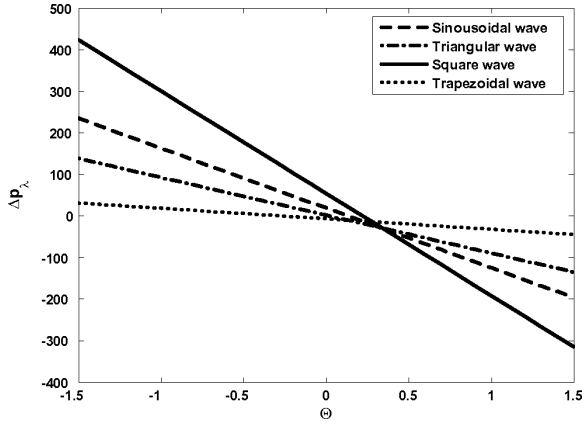

Fig. 15. Pressure rise versus flow rate for $\varepsilon = 0.45$, $a_1 = 0.4$, $\alpha = 0.8$.

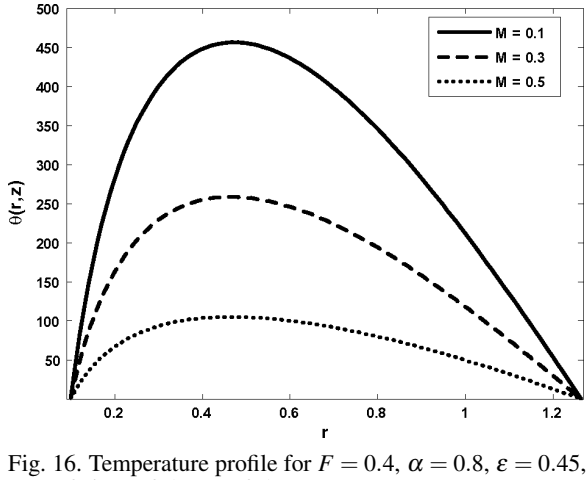

Fig. 16. Temperature profile for $F = 0.4$, $\alpha = 0.8$, $\varepsilon = 0.45$, $E_{\mathrm{m}} = 0.4$, $z = 0.1$, $a_1 = 0.1$.

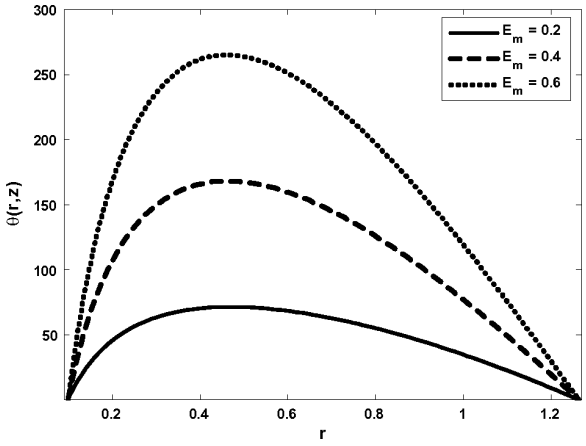

Fig. 17. Temperature profile for $F = 0.4$, $\alpha = 0.8$, $\varepsilon = 0.45$, $M = 0.4$, $z = 0.1$, $a_1 = 0.1$.

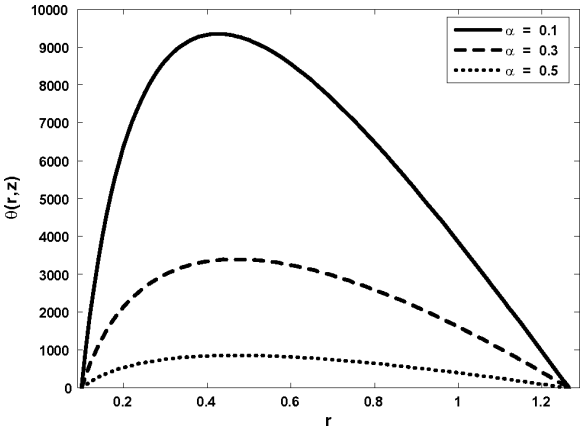

Fig. 18. Temperature profile for $F = 0.4$, $E_{\mathrm{m}} = 0.8$, $\varepsilon = 0.45$, $M = 0.4$, $z = 0.1$, $a_1 = 0.1$.

In this problem we will use the central difference approximation and replaced the derivatives by their discrete approximations

$$w'' = \frac{W_{i+1} - 2W_i + W_{i-1}}{(dr)^2}, \quad w' = \frac{W_{i+1} + W_{i-1}}{2(dr)}. \quad (36)$$

Using (36) in (34) and after rearranging, we get a system of algebraic equations

$$A_i W_{i+1} + BW_i + \mathrm{C}iW_{i-1} = D_i, \quad i = 1,2,3,\ldots,N.$$

Finally, the resulting tridiagonal system is solved by using the famous Thomas algorithm.

6. Numerical Results and Discussion

The main aim of the present work is to present the closed form solutions of an incompressible, magnetohydrodynamic Newtonian fluid through a porous horizontal annular region between two concentric tubes. A numerical solution of the problem has been also computed to discuss the validity and convergent of the two solutions which are presented in Figure 2. The expression for pressure and frictional forces per wave length are difficult to integrate analytically therefore numerical integration is used to evaluate the integrals. In Figures 3 – 6 the pressure rise is plotted versus the dimensionless flow rate Θ. In Figure 3, it is observed that pressure rise decreases with the increase in M up to $\Theta < 0.47$ and for $\Theta > 0.48$ it gives an opposite behaviour. The effects of the radius of the inner tube a_1 on pressure rise could be analyzed through Figure 4. It is seen that pressure rise increases with the increase in a_1 up to $\Theta < 0.48$, after that pressure rise decreases. Figure 4 is prepared to see the effects of α (Porosity parameter) on pressure rise versus flow rate. It is observed that pressure rise decreases with the increase in α up to $\Theta < 0.47$ and for $\Theta \geq 0.47$ it gives an opposite behaviour. Figure 6 shows the physical behaviour of the amplitude ratio ε on pressure rise. It is depicted from the figure that the pressure rise increases with the increase in ε up to $\Theta < 0.47$ and for $\Theta \geq 0.47$ it decreases. The frictionless force F_λ for inner and outer tube denoted by $F_\lambda^{(i)}$ and $F_\lambda^{(o)}$, respectively, are plotted in Figures 7 – 14. The region in which both, $F_\lambda^{(i)}$ and $F_\lambda^{(o)}$, are positive denotes the region where reflux phenomenon occurs and the region where $F_\lambda^{(i)}$ and $F_\lambda^{(o)}$ are negative designate to peristaltic pumping. We observed that the frictionless force has the opposite behaviour as compared to pressure rise. The expression for pressure rise per wavelength is evaluated numerically for the four considered wave forms and the result is presented graphically in Figure 5. It is observed from the graph that the square wave gives the best pumping characteristics among all wave forms. The trapezoidal wave has the worst pumping characteristics.

Figures 16 – 18 are prepared to see the effects of different parameters on the temperature profile. When we increase E_{m} the temperature profile increases while it decreases with the increase in α and M. The trapping phenomenon is an interesting phenomenon in peristaltic motion which is basically due to the circulation of the stream lines. We have discussed this phenomenon in Figures 20 – 23. Figures 20 and 21 show

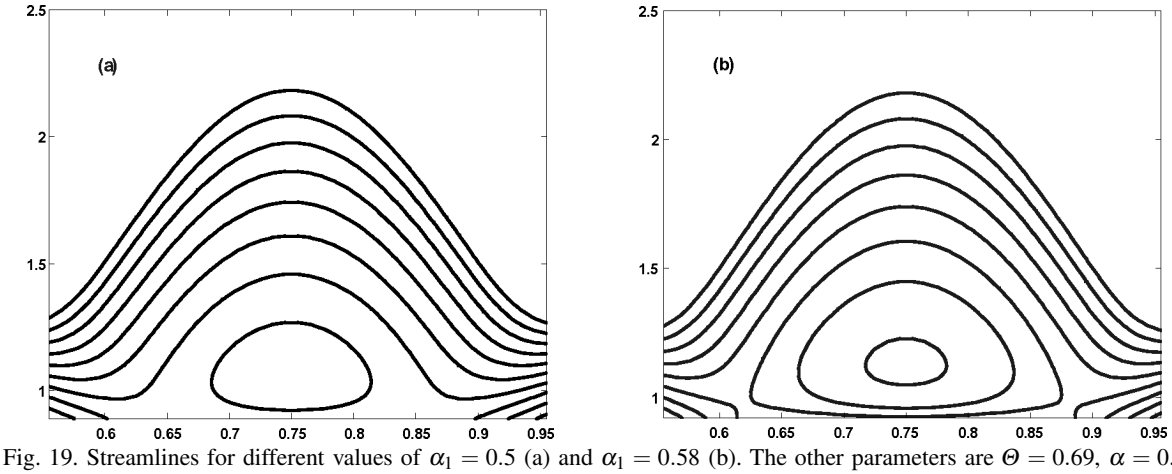

Fig. 19. Streamlines for different values of $\alpha_1 = 0.5$ (a) and $\alpha_1 = 0.58$ (b). The other parameters are $\Theta = 0.69$, $\alpha = 0.4$, $\varepsilon = 6.3$, $M = 1$.

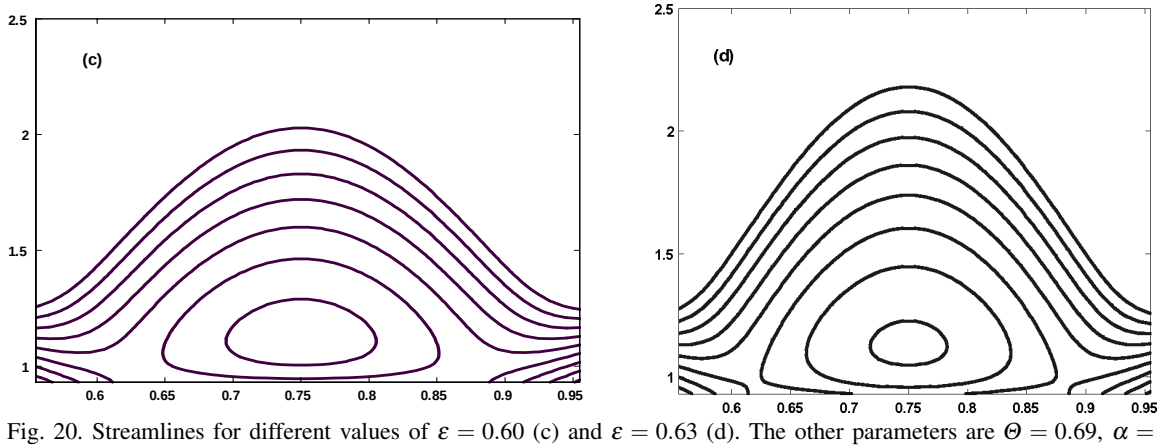

Fig. 20. Streamlines for different values of $\varepsilon = 0.60$ (c) and $\varepsilon = 0.63$ (d). The other parameters are $\Theta = 0.69$, $\alpha = 0.4$, $\alpha_1 = 0.51$, $M = 1$.

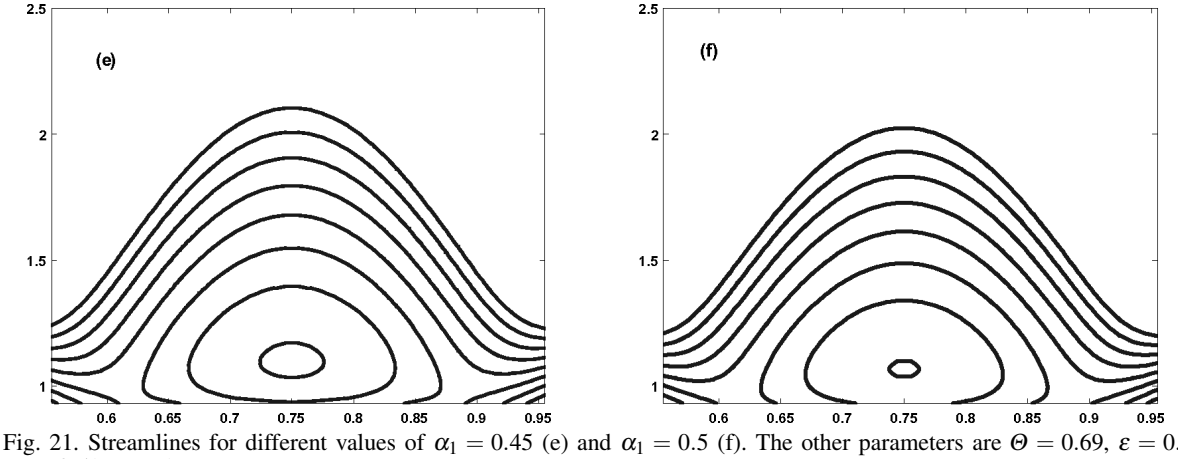

Fig. 21. Streamlines for different values of $\alpha_1 = 0.45$ (e) and $\alpha_1 = 0.5$ (f). The other parameters are $\Theta = 0.69$, $\varepsilon = 0.4$ $\alpha_1 = 0.51$, $M = 1$.

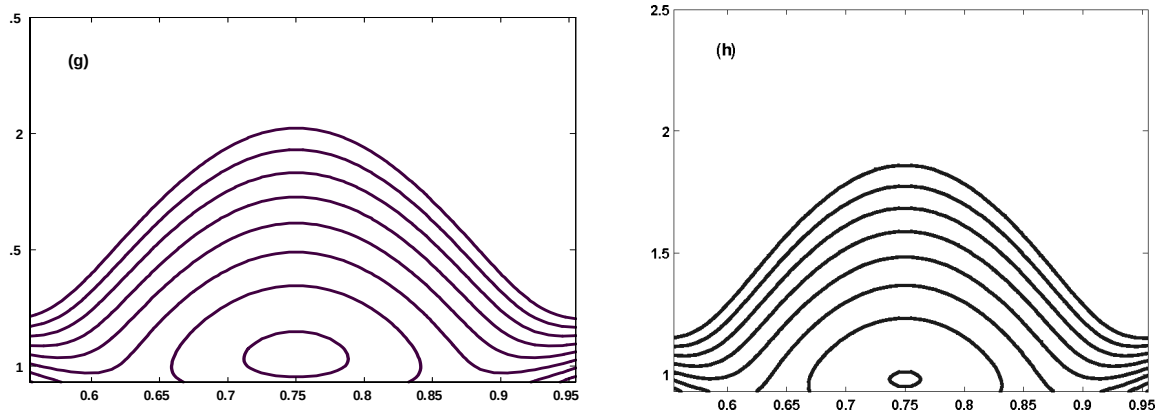

Fig. 22. Streamlines for different values of $M = 0.5$ (g) and $M = 0.8$ (h). The other parameters are $\Theta = 0.69$, $\varepsilon = 0.63$, $\alpha_1 = 0.55$, $\alpha = 1$.

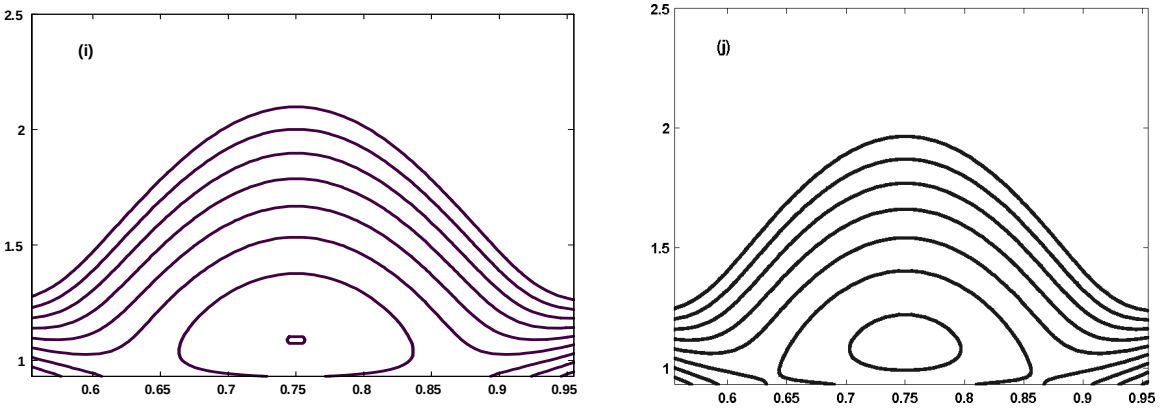

Fig. 23. Streamlines for different values of $\Theta = 0.68$ (i) and $\Theta = 0.7$ (j). The other parameters are $M = 0.4$, $\varepsilon = 0.6$, $\alpha_1 = 0.55$ $\alpha = 0.1$.

that with the increase in radius a_1 and amplitude ratio ε the size of trapped bolus decreases but the number of trapping bolus increases. Figures 21 and 22 shows that with the increase in α (Porosity parameter) and Hartmann number M the size of the trapped bolus decreases and the number of trapping bolus also decreases. Figure 23 shows that with the increase in flow rate Θ the size of trapped bolus increases.

[1] T. W. Latham, Fluid motion in a peristaltic pump, M. sc, Thesis, Massachusetts Institute of Technology, Cambridge 1966.
[2] L. M Srivastava and V. P Srivastava, J. Biomech. **17**, 821 (1982).
[3] V. Seshadri, Z. Hasan, and B. B. Gupta, J. Biophys. Med. Nucl. **8**, 9 (1984).
[4] S. Brasseur and N. Q. Lu, J. Fluid Mech. **174**, 495 (1987).
[5] M. Li and J. G. Brasseur, J. Fluid Mech. **248**, 129 (1993).
[6] J. C. Misra and S. K. Pandey, Appl. Math. Comput. **33**, 997 (2001).
[7] A. H. Abd El-Naby and A. E. M. El-Misiery, Appl. Math. Comput. **128**, 19 (2002).
[8] Kh. S. Mekheimer, Appl. Math. Comput. **153**, 763 (2004).
[9] D. S. Sankar and K. Hemalatha, Appl. Math. Modeling **31**, 1847 (2007).
[10] P. Hariharan, V. Seshadri, and R. K. Banerjee, Math. Comput. Modeling, **48**, 998 (2008).
[11] T. Hayat, N. Ahmed, and N. Ali, Commun. Nonlinear Sci. Numer. Simul. **13**, 1581 (2008).

[12] M. Kothandapani and S. Srinivas, Int. J. Nonlinear Mech. **43**, 915 (2008).
[13] T. Hayat and N. Ali, Commun. Nonlinear. Sci Numer. Simul. **13**, 1343 (2008).
[14] T. Hayat, Y. Wang, A. M. Siddiqui, K. Hutter, and S. Asghar, Math. Mod. Meth. Appl. Sci. **12**, 1691 (2002).
[15] Kh. S. Mekheimer and Y. Abd Elmaboud, Phys. A. **335**, 1 (2007).
[16] K. Vajravelu, G. Radhakrishnamacharya, and V. Radhakrishnamurty, Int. J. Nonlinear Mech. **42**, 754 (2007).
[17] S. Srinivas and M. Kothandapani, Int. Com. Heat Mass Trans. **35**, 514 (2008).
[18] R. C. Eberhart and A. Shitzer, Heat Transfer in Medicine and Biology, Analysis and Applications, Plenum Press, New York 1985.
[19] G. Radhakrishnamacharya and Ch. Srinivasulu, C. R. Mecanique **335**, 369 (2007).
[20] T. Hayat, M. U. Qureshi, and Q. Hussain, Appl. Math. Modelling **33**, 1862 (2009).
[21] N. T. M. Eldabe, M. F. El-Sayed, A. Y. Ghaly, and H. M. Sayed, Arch. Appl. Mech. **78**, 599 (2008).
[22] A. M. Wazawaz, Appl. Math. Comput. **123**, 109 (2001).
[23] A. M. Wazwaz, Appl. Math. Comput. **128**, 47 (2002).
[24] A. M. Wazwaz, Appl. Math. Comput. **61**, 543 (2005).
[25] E. F. Elshehawey, N. T. Eladabe, E. M. Elghazy, and A. Ebaid, Appl. Math. Comput. **182**, 140 (2006).
[26] N. T. Eldabe, E. M. Elghazy, and A. Ebaid, Phys. Lett. A **363**, 257 (2007).
[27] A. Ebaid, Phys. A **372**, 5321 (2008).
[28] S. Nadeem and N. S. Akbar, Commun. Nonlinear Sci. Numer. Simul. **14**, 3844 (2009).